# Ultrasonic Phased Array Imaging Technology for the Inspection of Aerospace Composite Structures

Reza Mohammadkhani
*School of Aerospace, Transport and Manufacturing*
*Cranfield University*
Cranfield, UK
r.mohammadkhani@cranfield.ac.uk

Luca Zanotti Fragonara
*School of Aerospace, Transport and Manufacturing*
*Cranfield University*
Cranfield, UK
l.zanottifragonara@cranfield.ac.uk

Janardhan Padiyar M.
*School of Aerospace, Transport and Manufacturing*
*Cranfield University*
Cranfield, UK
m.padiyar@cranfield.ac.uk

Ivan Petrunin
*School of Aerospace, Transport and Manufacturing*
*Cranfield University*
Cranfield, UK
i.petrunin@cranfield.ac.uk

Antonios Tsourdos
*School of Aerospace, Transport and Manufacturing*
*Cranfield University*
Cranfield, UK
a.tsourdos@cranfield.ac.uk

Iain Gray
*School of Aerospace, Transport and Manufacturing*
*Cranfield University*
Cranfield, UK
i.gray@cranfield.ac.uk

***Abstract*—In this article, we present the challenges and achievements in development and use of a compact ultrasonic Phased Array (PA) module and imaging technology for autonomous non-destructive evaluation of composite aerospace structures. We analyse the state of composite components by processing full waveform (A-scan) information from PA, perform slicing and visualization of the data.**

**We further accomplish the improvement of the axial (depth) resolution by proposing a new signal processing algorithm based on threshold improved wavelet transform (TIWT), that is able to separate overlapped echoes. This algorithm extracts a reference echo model from A-scans with no defect, and uses complex continuous wavelet transform and phase information of full waveform to estimate and localize echoes of each A-scan. The results of the proposed algorithm are validated by comparing them to the reference sample measures.**

***Index Terms*—CompInnova, Autonomous Inspections, Phased Array, Ultrasonic NDE, NDT, Composite**

## I. Introduction

This work is part of the H2020 CompInnova project that aims to develop an innovative solution for the automatic inspection, sizing, localization and repair of damages on aircraft composite structures [1], [2].

For the inspection phase, the CompInnova solution employs two different and complementary technologies: (i) Infrared Thermography (IRT) to detect near surface defects, and (ii) ultrasonic Phased Array (PA) for sub-surface defects. The combination of these two methods in the overlapping areas is also considered as the future work in CompInnova, in order to improve the accuracy of detection. These modules are meant to be mounted on a vortex robot for autonomous inspection of composite structures.

In this article, we focus on the challenges for the PA imaging technology that is an advanced non-destructive testing (NDT) method for in-service inspection and characterization of defects in and composite components. The use of autonomous systems for non-destructive testing has been explored by several authors in the literature using a wide range of sensing techniques. For instance, various robot inspectors have been designed and developed for the inspections of long welded lines [3] and a relatively recent literature review about climbing robots for inspections can be found in [4]. Similarly, Malandrakis et al. [5] postulated the use of unmanned aerial systems for the inspection of aircraft wing panels. Specifically, the use of phased array ultrasonics in autonomous inspections has been recently explored leveraging different technologies such as robotic manipulators [6], [7] and robots for in-pipe inspections [8], [9]. The aforementioned CompInnova concept [1] presents an integrated solution for automated inspection, defect recognition, sizing and repair of aerospace composite structures. The solution envisage to revolutionize the area of inspections for C and D checks, allowing faster repeatable inspections and accurate localization, sizing and classification of defects in a digit. Having these checks automated we can achieve a significant reduction in both costs and inspection time [2]. A vortex-based robotic platform [10] is the solution chosen for the PA and IRT inspectors. The use of a robotic platform for carrying out NDT ultrasonic inspections raises several technical questions and challenges. This paper is going

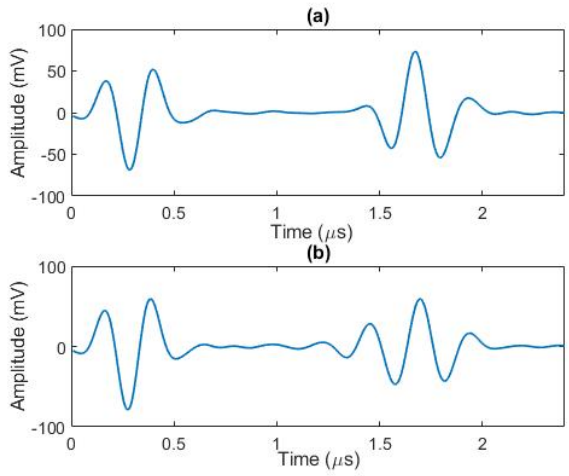


Fig. 1: A-scan data with (a) no defect, and (b) defect echo overlapping with backwall echo.

to address this and share the experience gained by the authors when dealing with this problem.

One of the main advantages of the PA inspection with full-waveform data capture and storage is the ability to re-analyze the data by adjusting the gate and retrieve the information about the depth of the defect. The depth information is crucial in the assessment of the defect, the state of the component and to decide whether repair, replacement or no-action is needed. In addition, for the CompInnova concept, the depth information is very valuable because it allows an accurate calculation of the volume and area of material that the laser during repair will remove.

Dead zone and limited axial resolution are the main draw backs related to the use of lower frequency PA ultrasonic transducer for defect detection and characterization of thin composite structures found in fuselages. The physical background of that limitation is related to the finite length of the wave packet transmitted into the material by the PA transducer. When the distance between the echoes in the analysed A-scan is comparable or less than the width of the wave packet, the separation of these two echoes becomes a challenging task for the operator or automation of damage detection.

The problem can be illustrated by the following examples. Let us consider a pristine case, characterized by A-scan shown in Fig. 1(a), where front-surface and back-wall echoes are clearly separated. In the presence of a defect, with a large distance from front-surface and backwall echoes (comparable or greater than the width of the wave packet), we can make a clear distinction between all echoes, i.e. localize each echo correctly.

However, when echoes are merging, for example Fig. 1(b) that shows an overlap between defect and back-wall echoes, proper localization is either not possible or will have a significant error by using conventional methods. Because of this phenomenon, the depth of defects close to the surface is difficult to estimate. In addition, even when there is no echo merging, due to the limited resolution of A-Scan signals, the defects in C-Scan from unprocessed A-Scans may appear to be much larger than the actual defects. In order to solve this problem, the axial resolution of A-Scan signals needs to be improved.

For example, given the velocity of longitudinal ultrasonic wave as 3 mm/s in a CFRP material and using 5, 10, and 15 MHz excitation frequencies, the wavelengths are 0.6, 0.3 and 0.2 mm respectively. For a layer thickness of 0.18 mm, we have a depth resolution for the above frequencies in C-scan approximately equal to the thickness of 3, 2, and 1 layers, respectively. We have observed that with 5 MHz frequency, we are able to detect and quantify the lateral extent of embedded inserts and impact damages in thin composites. But, we are not able to resolve individual plies for such frequency, and with no signal processing a transducer frequency over 10 MHz is needed.

However, increasing the frequency of PA transducer results in the increase of the ultrasonic attenuation and noise in the material. The scattering noise is due to wavelength being much closer to ply thickness, which causes internal reflections at each resin-ply interface and results in a train of continuous noise-like signatures between the front wall and back wall of the sample [11]. This noise is known as structural noise, which adds coherently as the ultrasound propagates in the material. Therefore, it is necessary to improve the resolution by dedicated signal processing.

This paper focuses on the development of the ultrasonic phased array imaging technology to provide 3D visualization and semi-automated characterization of near surface and far surface defects leveraging longitudinal full-waveform (A-scans) data captured by a portable PA hardware having 64 transducers with 0.8 mm pitch.

The remainder of this paper is organized as follows. In Section II, we present signal processing techniques to improve the performance of PA imaging and depth resolution. Then, results of our proposed algorithm using measured data for a reference standard specimen is discussed in Section III. Finally, Section IV concludes the paper.

## II. PA Imaging Technology

In this section, we present the development of a set of signal processing techniques to enhance the PA imaging performance by using axial resolution improvement, 3D visualization, slicing and sizing techniques to provide reliable 3D characterization of defects layer-by-layer.

### *A. Axial (depth) Resolution Improvement*

As discussed previously, the axial resolution depends on the frequency of the transmitted ultrasonic signal. Simplistically, the higher the frequency, the better the axial resolution. The axial resolution of a PA transducer also depends on the spatial extent (total pulse length) of the transmitted ultrasonic pulse through the wedge.

The pulse length of the signal coming out of the wedge is usually three or four wavelengths long. When defects are

located close to each other, their echoes merge. The accurate measurement of the depth of the impact damage requires the use of a transducer with higher frequencies, which have smaller pulse length.

For the axial resolution improvement, we developed a signal processing package that allows extracting a reference echo model from the A-scans with no defects. Having this reference echo model and using our proposed searching methods, each single echo of the original signal (A-scan) is approximated and subtracted from it one by one, until the remainder signal level is below a certain threshold. Figure 2 illustrates the flowchart of the algorithm, which is composed of the following steps:

- Compute the complex continuous wavelet transform of the signal x(t) to obtain the wavelet coefficients - scalogram $W(\tau, f)$;
- The maximum value in the scalogram $W(\tau, f)$ and its $\tau_W$ position is located over time axis;
- An echo estimate is created by scaling the reference echo model and shifting to $\tau_W \pm L$ (for a small $L$) to find the best possible approximate of the echo of x(t).
- The echo estimate is removed from the original signal and the maximum amplitude value in the remainder signal is found and compared to the threshold. If this is larger than the threshold, the resulting signal will become the input of the next iteration until the maximum value of the signal is smaller than the threshold.

The use of WT gives us more benefit (such as signal denoising and increasing signal to noise ratio) with our ongoing work at higher frequencies, namely 10 MHz.

Continuous wavelet transform can be presented in the form [12]:

$$W(a,b) = \frac{1}{\sqrt{a}} \int_{-\infty}^{+\infty} x(t)\psi^*(\frac{t-b}{a}))dt \qquad (1)$$

where $x(t)$ is a time domain signal; $\psi$ is the mother wavelet function; $a$ is the scale variable; $b$ is the time shift variable, and $^*$ denotes complex conjugation. In this study, the complex Morlet mother wavelet function is used:

$$\psi(t) = \frac{1}{\sqrt{\pi f_b}}(e^{j2\pi f_c t} - e^{-f_b(\pi f_c)^2})e^{\frac{-t^2}{f_b}} \qquad (2)$$

where $f_b$ is the bandwidth parameter, $f_c$ is the central frequency of the mother wavelet function, and $j$ is the imaginary unit.

For clarity and simplicity the results from the wavelet transform are presented in frequency rather than scale domain by converting corresponding scales to frequencies.

The threshold is defined as follows

$$\text{Threshold} = \frac{\alpha}{N} \sum_{n=1}^{N} |x(n)| \qquad (3)$$

where $\alpha$ is a scaling parameter to control the threshold and $N$ is the total number of samples of the original signal $x(n)$.

Results of performing the above procedure for the two cases of (i) having well-separated echoes and (ii) echoes with overlap, are shown in Figures 3(a) and 4(a). Comparing the results in Fig 3(b) and Fig 4(b), we can find the size of inserts and the relative depths by having $\tau_f$, $\tau_d$ and $\tau_b$ as the location of front-surface, defect and back-wall echoes in time, respectively, and knowing the velocity of sound in the material. For example, the thickness of the sample with no inserts from Fig. 4 can be calculated as

$$x = v(\tau_b - \tau_f)/2 = 2.1 \text{ mm}. \qquad (4)$$

Similarly, we can obtain the defect depth by using $\tau_d$ instead of $\tau_b$ as 1.8 mm for the sample with insert in Fig. 4. However, thickness of the sample is varied between 2.1 mm and 2.3 mm from different A-scans with defects. Having the insert thickness less than 0.1 mm, and each layer thickness of 0.183 mm, and knowing that each insert is placed between layer 10 and 11, the above measures are reasonable. However, the small variation in depth information might be due to the velocity approximation, and manufacturing tolerance.

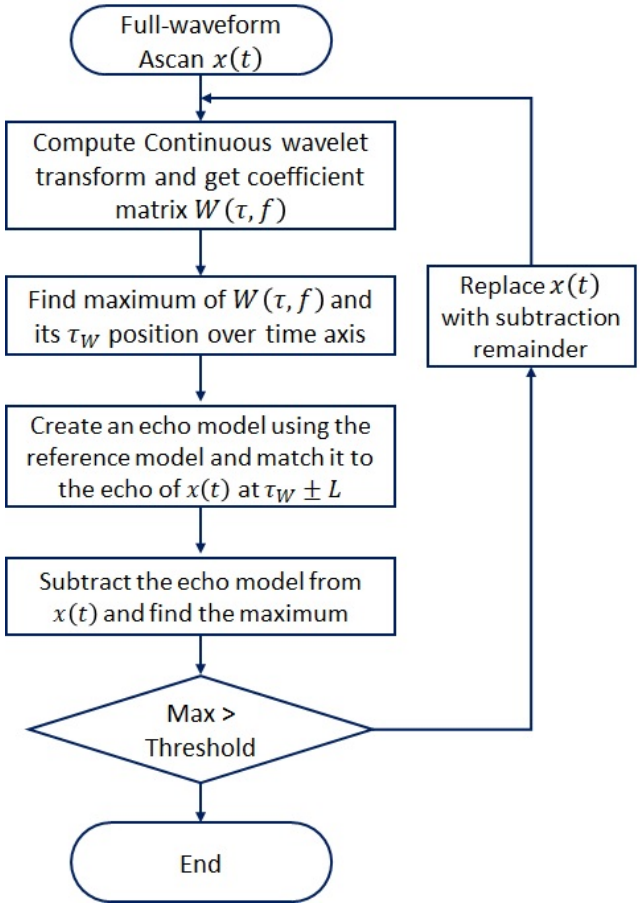


Fig. 2: Flowchart of our algorithm that improves the axial resolution.

### *B. Slicing and 3D visualization of data*

The proposed algorithm is capable of extracting the defect depth and of defining the slices size which can be set, conveniently, equal to thickness of the composite layer. Detection is performed in each slice separately based, for

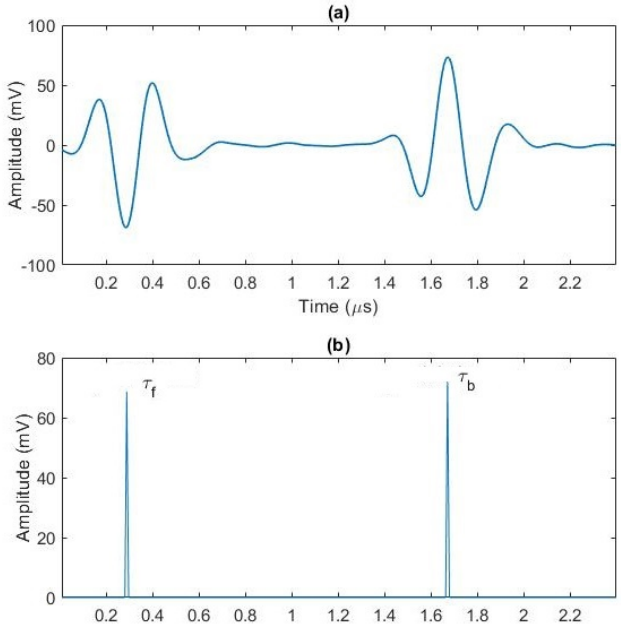


Fig. 3: (a) Full waveform A-scan with no defect, and (b) localized front-surface and backwall echoes in time.

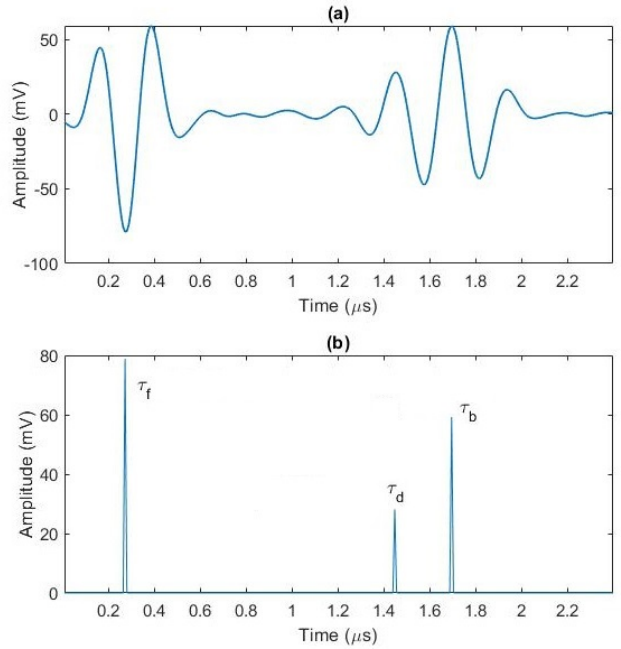


Fig. 4: (a) Full waveform A-scan with overlap between defect and backwall echoes, (b) localized echoes using our algorithm.

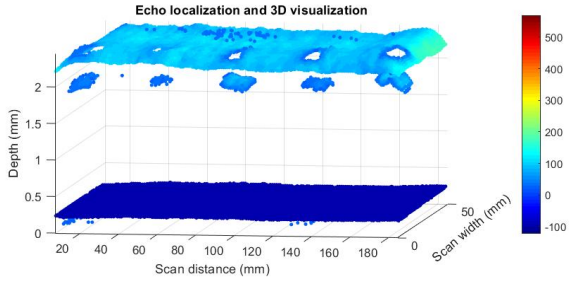


Fig. 5: Alignment, echo localization and 3D visualization of $12 \times 12$ mm FOD with $\alpha = 1.6$.

example, on amplitude information. The depth of the zone is calculated according to time of flight information and a 3D plot containing detected defects from each zone/slice is created. Using this technique it is possible to quantify the defects layer-by-layer. This information is then fed into the characterization software, which is not presented in this paper, that can estimate geometry of the defect at each layer of the material and can be used for planning the repair phase.

In order to provide a clearer view for the inspector on the defect profile over the material depth, a visualization function has been implemented. The layers with defects that have been recognized by the slicing algorithm are fed into the visualization function. In this paper we use the minimum possible thickness of the slice, limited by discrete presentation of the signal. Fig. 5 illustrates how this function visualizes 3D plot of material volume. The PA inspection is carried out using a linear scanning method, where the beam is swept electronically (without focusing) using an optimum active aperture. By active aperture or probe aperture we mean a group of adjacent transducers are excited simultaneously (limited by the PA hardware)

Fig. 6 shows an example of visual results our from signal processing package that provides a 3D plot of defect detection for each layer of composite material as a result of slicing and resolution improvement.

## III. Results and Discussion

We post-process and analyse full waveform ultrasonic signals. The PA inspection is carried out using a linear scanning method, where the beam is swept electronically (without focusing) using an optimum active aperture. After careful examination, an active aperture of 8 elements is chosen for our scenario. Therefore, we have (64-8+1) = 57 different A-scans along the line of the transducer elements that can be controlled electronically. By analyzing these A-scans along x-axis, we have a 2D image perpendicular to the surface of the sample, which is called B-scan. However, to complete a top-view image of the specimen, or C-scan, we need to move the PA mechanically. This movement along the y-axis is captured by the encoder with resolution of 1 mm. The full waveform data captured is converted from Sonatest OEM format to CSV for further processing.

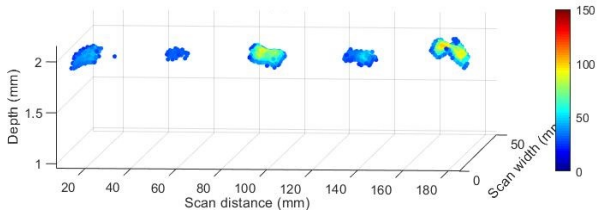


(a)

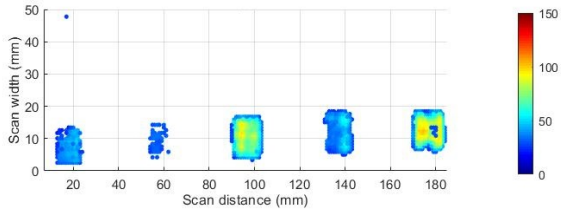


(b)

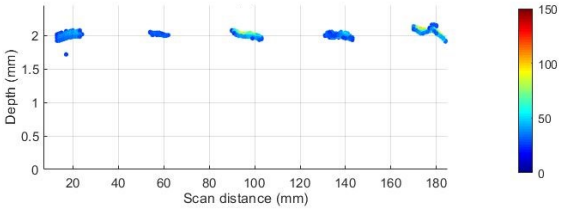


(c)

Fig. 6: (a) 3D visualization of echo localization that provides (b) size, and (c) depth information of $12 \times 12$ mm FOD with $\alpha = 1.3$.

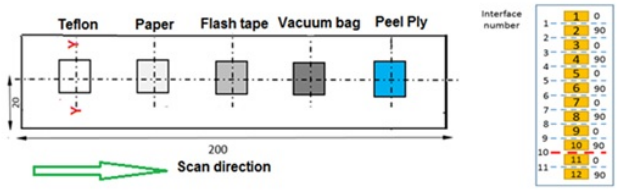


Fig. 7: Schematic of the reference standard specimen with different material inserts at the same depth, between layers 10 and 11.

As shown in Fig. 7, a twelve layered CFRP specimen [0/90]3s with an average total cured thickness of 2.3 mm, is used for PA imaging as the reference standard specimen, having five different material inserts as artificial defects, to represent both tight delamination-type defects and Foreign Object Defects (FOD). All inserts have the same size (mm-by-mm) and they are placed at the same depth (e.g., between layers 10 and 11 for the following measurements).

Figures 9 and 8 illustrate amplitude-based and ToF-based C-scan images for the two sizes $12 \times 12$ mm, and $3 \times 3$ mm of FOD inserts, provided by an ultrasonic NDT technician expert, before applying our proposed signal processing algorithm. Here, we have no depth information for the defects, and size information for inserts should be calculated manually.

Figures 5 and 6 demonstrate the performance of our signal

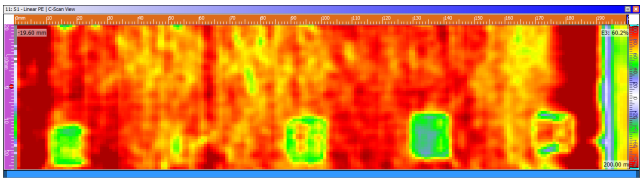

(a)

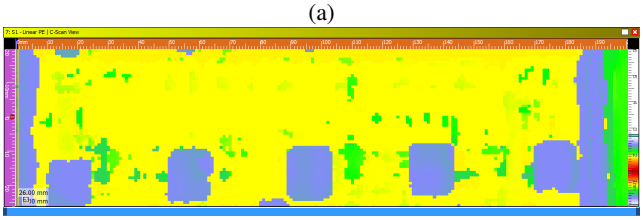

(b)

Fig. 8: (a) Amplitude-based and (b) time-of-flight (ToF) based C-scan images of $12 \times 12$ mm FOD of different materials at the same depth, between layers 10 and 11, in the reference standard specimen, with the scan direction shown in Fig. 7.

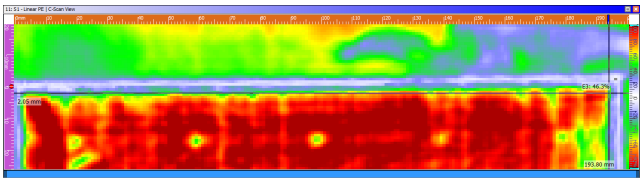

(a)

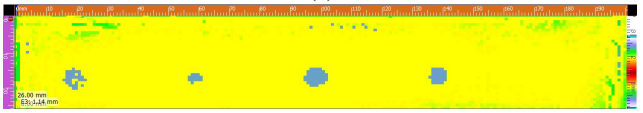

(b)

Fig. 9: (a) Amplitude-based and (b) time-of-flight (ToF) based C-scan images of $3 \times 3$ mm FOD of different materials at the same depth, between layers 10 and 11, in the reference standard specimen. However, the scan direction is opposite to what is shown in Fig. 7.

TABLE I: Manual size* detection from the PA hardware output with no depth information, compared to size (mm×mm) and depth (mm) information using our proposed algorithm for different types of $12 \times 12$ mm inserts.

| | Teflon | Paper | Flash tape | Vacuum bag | Peel ply |
|---|---|---|---|---|---|
| size* | $15.5 \times 13.5$ | $14 \times 14.5$ | $15 \times 15$ | $14.5 \times 16$ | $14 \times 14$ |
| size | $10 \times 11$ | $7 \times 10$ | $13 \times 12.5$ | $12 \times 12.6$ | $14 \times 11.7$ |
| depth | 1.68-1.83 | 1.75-1.80 | 1.69-1.83 | 1.70-1.79 | 1.67-1.90 |

TABLE II: Size (mm×mm) and depth (mm) information for different types of $3 \times 3$ mm inserts using our proposed algorithm.

| | Teflon | Paper | Flash tape | Vacuum bag | Peel ply |
|---|---|---|---|---|---|
| size | - | $5 \times 3.3$ | $5 \times 3.4$ | $3 \times 1.6$ | $5 \times 4.2$ |
| depth | - | 1.67-1.73 | 1.68-1.69 | 1.68-1.69 | 1.69-1.75 |

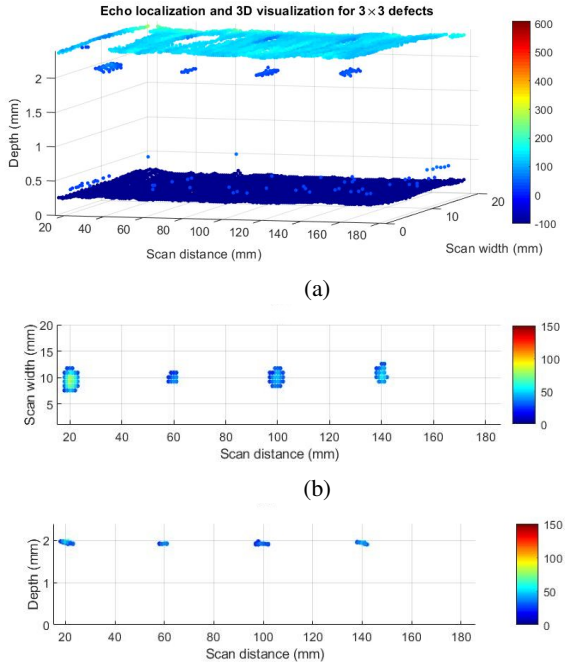


Fig. 10: (a) Alignment, Echo localization and 3D visualization of $3 \times 3$ mm FOD, and our algorithm can provide (b) size, and (c) depth information.

processing package for $12 \times 12$ mm defects. All echoes are localized in Figure 5 with two planes at the bottom and top, representing front-surface and back-wall echoes, respectively. Therefore, any depth information is considered related to the position of front-surface echoes at 0.24 mm. By using the proposed algorithm we quantified the depth information for the defects in Fig. 6 providing more clear and easy to understand information compared to the results in Fig. 9. Table I compares the performance of our proposed algorithm with the manual size calculation using output data from our PA hardware. As we see, our algorithm provides more accurate size information, in addition to the depth information.

We further investigate the performance of our algorithm by considering $3 \times 3$ mm FOD inserts in Fig. 10. We observe that our algorithm detects the position, size and depth information of small size defects close to the backwall, except Teflon insert. We further see that size detection depends on the type of insert and our algorithm is detecting size of other types of inserts, with a reliable depth information.

## IV. Conclusion

In this paper we analyzed the challenges of having an ultrasonic PA module in an autonomous inspection platform designed for the NDT of aerospace composite structures. We developed a signal processing package, utilizing a new threshold improved wavelet transform (TIWT) algorithm, to provide novel volume visualization solution for damage quantification. This algorithm is also able to resolve overlapped echoes by extracting a reference echo model from the measurement data (A-scans) and to provide reliable depth information. Having a ground truth measurement obtained from the calibration sample, we could confirm the validity and quantify the resolution improvement results of our algorithm having different types of inserts and two sizes of $12 \times 12$ and $3 \times 3$.

## Acknowledgement

The authors wish to acknowledge the funding contribution from the European Union's H2020 Framework Programme, call FET-OPEN under REA grant agreement No 665238 CompInnova. We also would like to thank the research group of Prof. V. Kostopoulos, Laboratory of Applied Mechanics and Vibrations, University of Patras, Greece for providing the CFRP samples.

## References

[1] I. Gray, M. J. Padiyar, I. Petrunin, J. Raposo, L. Zanotti Fragonara, *et al.*, "A Novel Approach for the Autonomous Inspection and Repair of Aircraft Composite Structures," *18th Eur. Conf. Compos. Mater.*, Athens, Greece, June 24-28, 2018.

[2] V Kostopoulos, S Psarras, T Loutas, G Sotiriadis, *et al.*, "Autonomous Inspection and Repair of Aircraft Composite Structures," *IFAC-PapersOnLine*, vol. 51, no. 30, pp. 554-557, 2018.

[3] J. Shang, B. Bridge, T. Sattar, S. Mondal, and A. Brenner, "Development of a climbing robot for inspection of long weld lines," *Ind. Robot An Int. J.*, vol. 35, no. 3, pp. 217-223, May 2008.

[4] D. Schmidt and K. Berns, "Climbing robots for maintenance and inspections of vertical structuresA survey of design aspects and technologies," *Rob. Auton. Syst.*, vol. 61, no. 12, pp. 1288-1305, Dec. 2013.

[5] K. Malandrakis, A. Savvaris, J.A.G. Domingo, N. Avdelidis, *et al.*, "Inspection of aircraft wing panels using unmanned aerial vehicles," *5th IEEE Int. Work. Metrol. AeroSpace, Metroaerosp. 2018 Proc.*, pp. 56-61, June 2018.

[6] C Mineo, C MacLeod, M Morozov, *et al.*, "Fast ultrasonic phased array inspection of complex geometries delivered through robotic manipulators and high speed data acquisition instrumentation," in *2016 IEEE International Ultrasonics Symposium, IUS*, pp. 1-4, Nov 2016.

[7] C. Mineo, R. Summan, J. Riise, C. N. MacLeod, and S. G. Pierce, "Introducing a new method for efficient visualization of complex shape 3D ultrasonic phased-array C-scans," in *2017 IEEE International Ultrasonics Symposium (IUS)*, pp. 1-4, 2017.

[8] H.J. Zhong, Z.W. Ling, C.J. Miao, W.C. Guo, and P. Tang, "A New Robot-Based System for In-Pipe Ultrasonic Inspection of Pressure Pipelines," in *2017 Far East NDT New Technology and Application Forum (FENDT)*, pp. 246-250, 2017.

[9] M. Švejda, "New Robotic Architecture for NDT Applications," *IFAC Proc.*, vol. 47, no. 3, pp. 11761-11766, Jan. 2014.

[10] G. Andrikopoulos and G. Nikolakopoulos, "Vortex Actuation via Electric Ducted Fans: an Experimental Study," *J. Intell. Robot. Syst.*, pp. 1-19, Sep. 2018.

[11] R. A. Smith, D. A. Bruce, L. D. Jones, A. B. Marriott, *et al.*, "Ultrasonic C-Scan Standardization for Polymer-Matrix Composites - Acoustic Considerations," in *Review of Progress in Quantitative Nondestructive Evaluation*, Springer, pp. 2037-2044, 1998.

[12] L. Gelman, I. Petrunin, I. K. Jennions, and M. Walters, "Diagnostics of local tooth damage in gears by the wavelet technology." *Int J Progn Health Manag*, vol. 3, no. 5, pp. 1-7, 2012.